Chemosphere 350 (2024) 141050

Contents lists available at ScienceDirect

Chemosphere

journal homepage: www.elsevier.com/locate/chemosphere

Reactive transport model for bentonites in COMSOL multiphysics: Benchmark and validation exercise

Virginia Cabrera [1], Rubén López-Vizcaíno [*], Ángel Yustres [*], Vicente Navarro

Geoenvironmental Group, Department of Civil Engineering and Construction, Civil Engineering School, University of Castilla-La Mancha, Ciudad Real, Spain

HIGHLIGHTS

- New reactive transport model for bentonites implemented in COMSOL Multiphysics.
- Model includes a complex geochemical system composed of 42 species and 4 minerals.
- Diffusive-dispersive-advective transport in double-porosity media is considered.
- Model verified and validated using a benchmark based on multicomponent infiltration.

GRAPHICAL ABSTRACT

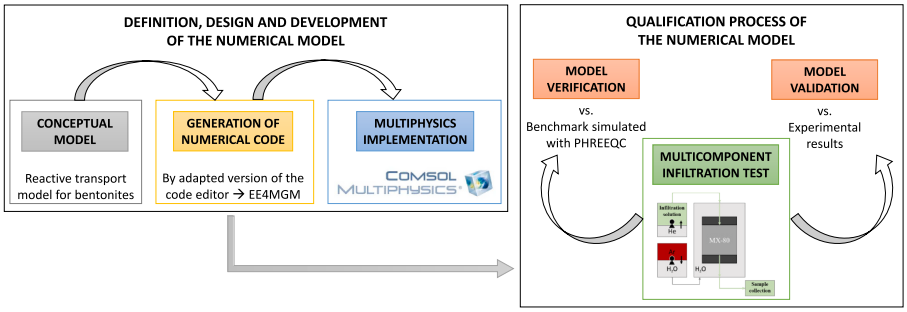

ARTICLE INFO

Handling editor: Milena Horvat

Keywords:
Bentonite
MX-80
Reactive transport
COMSOL
Benchmark
Infiltration test

ABSTRACT

At present, the deep geological repository concept for spent nuclear fuel is considered the most reliable and safe technique for the permanent disposal of this type of waste. One of the many safety elements used is an engineered barrier made of compacted bentonite. This material allows the encapsulated waste to be isolated from the host rock. Therefore, there is great interest in a detailed study of the behavior of bentonites to different changes in the composition of the surrounding groundwater.

In this context, this work presents a new reactive transport model for bentonites implemented in the COMSOL Multiphysics platform. The model contemplates a non-simplistic geochemical system composed of 42 species and 4 minerals. Reactive transport involves the diffusive-dispersive-advective processes defined by the Nernst Planck equations for two overlapping modeling levels (macro- and microstructural) to simulate the behavior of double-porosity media. The uniqueness of this model is that the system of equations used to calculate the chemical speciation problem and the advective-diffusive-dispersive transport can be integrally solved in COMSOL. The model has been satisfactorily verified and validated using the benchmark exercise consisting of the simulation of the multicomponent advective-diffusive column experiment conducted on a compacted bentonite core extracted from a field experiment (LOT project) in the Äspö Hardrock laboratory (Sweden).

* Corresponding authors. Geoenvironmental Group, Department of Civil Engineering and Construction, Civil Engineering School, University of Castilla-La Mancha, Avda. Camilo José Cela s/n, 13071, Ciudad Real, Spain.

E-mail addresses: ruben.lopezvizcaino@uclm.es (R. López-Vizcaíno), angel.yustres@uclm.es (Á. Yustres).

[1] Amphos 21 Consulting, Barcelona, Spain (Present Address).

https://doi.org/10.1016/j.chemosphere.2023.141050
Received 11 September 2023; Received in revised form 18 December 2023; Accepted 26 December 2023
Available online 26 December 2023
0045-6535/© 2024 The Authors. Published by Elsevier Ltd. This is an open access article under the CC BY-NC-ND license (http://creativecommons.org/licenses/by-nc-nd/4.0/).

1. Introduction

Different strategies are being considered for the construction of deep geological repositories for spent nuclear fuel (IAEA, 2020). Active clays, mainly compacted bentonites, have been selected as one of the fundamental engineering barrier elements. These materials present an advantageous collection of properties for waste-containment technology, such as low hydraulic conductivity, high swelling potential and high retention capacity (Pusch, 1992, 2006; Sellin and Leupin, 2014). Compacted bentonite is usually employed both for buffer and for backfill elements and is located in crystalline and argillaceous host rock. At present, the properties and behavior of several compacted bentonites are being analyzed, and among the most studied could be MX-80 (Villar et al., 2005; Karnland et al., 2006; Kiviranta and Kumpulainen, 2011; Toprak et al., 2013; Kiviranta et al., 2018).

The interaction between the porewater of bentonite and the surrounding groundwaters in deep geological repositories is a relevant topic of study (Karnland et al., 2005; Zhu et al., 2013; Wersin et al., 2016). In many studies, evidence of changes in hydromechanical properties linked to changes in porewater chemistry have been presented. Swelling pressure and hydraulic conductivity are affected in the case of very high salinities, and very low salinities may favor colloidal erosion (Posiva, 2012b). Moreover, the evolution of the pore water chemistry can decrease the isolation capacity and, in the case of canister failure, may also cause a decrease in the radionuclide retention capacity, which is a key issue in the long-term stability of bentonite barriers (Posiva, 2012a). Therefore, both the expected evolution and unlikely events impairing long-term safety must be analyzed. Groundwaters should account for chemically different scenarios, such as the water derived from ice melting at the end of a glacial period and the high-saline fluid of deep-seated brines, not only the present-day groundwater. Changes in groundwater chemistry can modify the dissolution-precipitation of carbonate minerals and gypsum, the oxidative dissolution of pyrite and iron oxyhydroxide, cation exchange and surface protonation-deprotonation, among other reactive processes (Arcos et al., 2008). These aspects, together with the complex geochemical system of MX-80 (Kiviranta and Kumpulainen, 2011), make it necessary to develop reactive transport models that involve these chemical processes (Steefel et al., 2015). The models complement the valuable results obtained in several long-term tests, many of which were conducted in underground research laboratories under operational conditions similar to those of an actual deep geological repository (Delay et al., 2014; Bildstein and Claret, 2015; Claret et al., 2018; Bildstein et al., 2019; Deissmann et al., 2021).

In this context, a reactive transport model for bentonites implemented in the multiphysics platform COMSOL (COMSOL, 2018) is presented in this work. This kind of multiphysics platform has been used, generally to develop reactive transport models coupled with other software to solve the geochemical speciation problem by the operator splitting approach (Carrayrou et al., 2004; Jacques et al., 2006). A highlight novelty of the presented model is that the system of equations used to calculate the chemical speciation problem and the advective-diffusive-dispersive transport can be integrally solved in COMSOL (monolithic approach). The multiphysics code editor EE4MGM (López-Vizcaíno et al., 2021) has been used to implement the geochemical model into the COMSOL platform. This strategy offers several advantages. The computational time is reduced by avoiding the need to reset the geochemical module and read the thermodynamic database at each time step. Additionally, the time required for data exchange between the transport and chemical reaction modules is eliminated. Moreover, potential errors in managing transient boundary conditions and mass balance errors associated with selecting the correct calculation time step can be eliminated (Barry et al., 1997; Carrayrou et al., 2004; Jacques et al., 2006). Furthermore, the COMSOL platform allows working at the level of defining the coefficients of the partial differential equations (PDEs), with the solution left to the symbolic algebra and numerical algorithms included in the software (Farrell et al., 2013; McRae et al., 2016; Houston and Sime, 2018). This provides great flexibility to the end user for modeling complex problems quickly and efficiently (López-Vizcaíno et al., 2017; Navarro et al., 2019).

The benchmark selected to verify the proposed model was based on the exercise published by Alt-Epping et al. (2015), which consisted of 5 problems of increasing complexity: (i) first, simulation of transport only, (ii) next, implementing the reaction network, (iii) adding conventional ion exchange, (iv) implementation of electrical double layer (EDL) and (v) inclusion of surface complexation process. The codes evaluated were CrunchFlow (Steefel et al., 2015), PHREEQC (Parkhurst and Appelo, 2013), MIN3P (Mayer, 2010) and FLOTRAN (Lichtner, 2007). Specifically, in this work, the fourth problem that considers the effect of the surface charge of montmorillonite on the distribution of species and their transport was selected and PHREEQC was used as the reference software. The benchmark exercise consists of the simulation of the multicomponent advective-diffusive column experiment conducted on a compacted bentonite core extracted from a field experiment conducted under LOT project (Karnland et al., 2009). The LOT project involves multiple test series to examine the interaction between a bentonite buffer composed of MX-80 and a granitoid host rock in an experimental repository at the Äspö Hardrock laboratory (Sweden). The selected infiltration experiment was carried out by the Rock–Water Interaction Group at the Institute of Geological Sciences of the University of Bern (Fernández et al., 2011; Jenni et al., 2014). In addition, after completing the verification process, the proposed model was validated. For this purpose, the results obtained with the numerical tool were contrasted with the experimental data of the infiltration test corresponding to the benchmark. In this context, this article is structured in different sections. Firstly, the conceptual model adopted is presented in detail, as well as the mathematical model used to solve the reactive transport problem studied. Then, the implementation process of the model is illustrated, followed by the description of the simulated experimental test. Finally, the most relevant results of the verification and validation process are presented.

2. Reactive transport model

The conceptual model selected for the functional structure of compacted bentonite is based on a double-porosity approach, as applied by other authors (Gens and Alonso, 1992; Mašín, 2013; Navarro et al., 2015). This approach assumes the internal structure of clays as two coupled and superimposed continua from a macroscopic point of view (Hueckel, 1992). One of these continua corresponds to the microstructural modeling level, which is determined on the support of the clay particle aggregates (intra-aggregate level). On the other hand, the support of the remainder of the interaggregate space is involved in the macrostructural modeling level (Alonso and Navarro, 2005). The type and size of pores defined by each modeling level are aspects that are not clearly defined since there is no rigid range to define the diameter of the pores included in each level. Even so, as many authors have suggested (Gens and Alonso, 1992; Alonso et al., 1999; Romero et al., 1999, 2011; Sánchez et al., 2005; Romero, 2013), the internal arrangement of clays is based on the assumption of these two modeling levels. The microstructural voids are linked to the diffusive layer (DL), and the macrostructural pores correspond to the volume that contains the free water (FW).

The negative net electrical charge of the clay particles involves several thermodynamic, chemical, and electrical effects that are associated with the microstructural modeling level. Considering these aspects, in this work, it is assumed that (i) the microstructural water is not affected by conventional hydrodynamic gradients and therefore, Darcian flux is not produced at this level, (ii) electrostatic effects are mainly produced at the microstructural level, generating a different average electrical potential from that present at the macrostructural level and (iii) the macrostructural pore water (FW) is electrically neutral (Appelo

and Wersin, 2007; Gimmi and Alt-Epping, 2018; Yustres et al., 2020).

2.1. Chemical speciation at the macrostructural modeling level

Assuming that the geochemical system is composed of I species classified in S secondary species, which are the reaction products of the combination of M ($=I–S$) master species or components (Bethke, 2007), the total concentration of the m-th master species in the macrostructural modeling level (determined by superscript M), C_m^M, is defined as:

$$C_m^M = \sum_{i=1}^{I} \alpha_{im} c_i^M \tag{1}$$

where c_i^M is the molal concentration of the i-th species in macrostructural water and α_{im} is the stoichiometry coefficient of the m-th master species involved in the chemical reaction of formation of the i-th species (López-Vizcaíno et al., 2017). When the m-th species is a reactant, the value of α_{im} will be positive and negative if it is a product. The molal concentration of the i-th species is obtained from the activity definition $a_i^M = \gamma_i^M c_i^M$, where a_i^M and γ_i^M are the activity and the activity coefficient of the i-th species in the macrostructure, respectively.

Two different approaches have been used to calculate the activity coefficient in the macrostructure depending on the charge of the i-th species. The LLNL (Lawrence Livermore National Laboratory) model (Daveler and Wolery, 1992) was selected for charged species and the parameterization proposed by Drummond (1981) was selected for the activity coefficients of uncharged species.

The generic chemical equilibrium equation was used to calculate the activity of each i-th species:

$$\log_{10}(a_i^M) = \log_{10}(K_{eq,i}) + \sum_{m=1}^{M} \alpha_{im} \log_{10}(a_m^M) \tag{2}$$

where $K_{eq,i}$ is the equilibrium constant of the chemical reaction of the i-th species formation by the combination of the m-th master species and a_m^M is the activity of each m-th master species in the macrostructure. The model contemplates the temperature dependence of $K_{eq,i}$.

The water activity in the macrostructure, $a_{H_2O}^M$, is defined as (Parkhurst and Appelo, 2013)

$$a_{H_2O}^M = 1 - 0.017 \sum_{i=1}^{I-H_2O} c_i^M \tag{3}$$

where the summation involves the concentrations of all the i-th species except that of H_2O itself. In addition, the ionic strength is calculated as follows:

$$I_S = \frac{1}{2} \sum_{i=1}^{I} c_i^M z_i^2 \tag{4}$$

2.2. Chemical speciation at the microstructural modeling level

The model assumes that the water contained in the microstructural modeling level or microporosity corresponds with the water in the double diffuse layer (DDL) and in turn with the Donnan space (Appelo and Wersin, 2007; Alt-Epping et al., 2015; Gimmi and Alt-Epping, 2018). For this purpose, the relation between the Donnan distance, d_D, and the microstructural void ratio, e^m, must be fulfilled as:

$$d_D = \frac{e^m}{\rho_s \, SSA} \tag{5}$$

where SSA is the specific surface area of the clay and ρ_s is the density of the solid particles.

In this context, the Donnan equilibrium approach has been assumed between both modeling levels (electrochemical potential is equal at the microstructure and macrostructure). This allows us to calculate the concentration of the i-th species in the microstructure as a function of the chemical composition in macrostructural water (free or bulk water) by the following expression (Gimmi and Alt-Epping, 2018):

$$c_i^m = c_i^M \exp\left(\frac{-z_i F \psi_D}{RT}\right) \tag{6}$$

where c_i^m is the concentration of the i-th species at the microstructural level, F is the Faraday constant, R is the gas constant and ψ_D is the Donnan potential generated between micro- and macrostructural waters due to the electrostatic effects generated by the negative charge of clay particles. Eq. (12) implies that the activity coefficients are equal at the micro- and macrostructural levels ($\gamma_i^m = \gamma_i^M$), as in (Alt-Epping et al., 2015). Donnan's theory includes the requirement of the electroneutrality condition at both modeling levels (Tournassat and Appelo, 2011). At the macrostructural level, the following equation must be fulfilled:

$$\sum_{i=1}^{I} z_i c_i^M = 0 \tag{7}$$

On the other hand, the electroneutrality condition at the microstructural level is presented as:

$$\sum_{i=1}^{I} z_i c_i^m + Q = 0$$

where z_i correspond to the charge number and Q is the charge concentration of clay particles defined as:

$$Q = \frac{\rho_s}{e^m} CEC \tag{8}$$

where CEC is the cation exchange coefficient.

2.3. Mass balance of species at both modeling levels

To define the spatial and temporal evolution of each m-th master species, it was necessary to solve the mass balance defined by the following equation:

$$\frac{\partial m_m}{\partial t} + \nabla \mathbf{J}_m - f_m = 0 \tag{9}$$

where m_m is the total mass per unit of volume, $\mathbf{J}_m$ is the total flux and f_m is the sink/source term of the m-th species. The total mass of the m-th species is composed of the contribution of the mass in the structural levels contemplated, m_m^L, where superscript L denotes the modeling level ("M" in macrostructure and "m" in microstructure). The total mass in the L-th modeling level is defined as:

$$m_m^L = C_m^L Sr^L \varphi^L \tag{10}$$

where C_m^L is the total concentration of the m-th master species, Sr^L is the degree of saturation and φ^L is the porosity evaluated by the three variables at level L. The total concentration of the m-th master species at the microstructural modeling level, C_m^m, is calculated using an expression such as Eq. (1) depending on c_i^m. The microstructure is assumed to be fully saturated; therefore, the degree of saturation in the microstructure is $Sr^m = 1$).

2.3.1. Transport of species at both modeling levels

The total flux is composed of the contribution of two phenomena: (i) advection and (ii) diffusive-dispersive transport. The first transport mechanism, advection, is only produced at the macrostructural level ($\mathbf{J}_{adv,m}^M$) because, as previously mentioned, microstructural water is not influenced by hydrodynamic gradients (Darcian flux = 0). On the other hand, diffusive-dispersive transport takes place at both modeling levels

($\mathbf{J}^{M}_{dif-dis,m}$ in macrostructure and $\mathbf{J}^{m}_{dif-dis,m}$ in microstructure) (Alt-Epping et al., 2015). Taking into account these aspects, $\mathbf{J}_m$ is defined following the extended Nernst–Planck equation (Rasouli et al., 2015; Rolle et al., 2018; Sprocati et al., 2019) as:

$$\mathbf{J}_m = \mathbf{J}^{M}_{adv,m} + \mathbf{J}^{M}_{dif-dis,m} + \mathbf{J}^{m}_{dif-dis,m} = \left(C^{M}_{m} q^{M}_{adv}\right) + \left(\sum_{i=1}^{I} \alpha_{im} \mathbf{j}^{M}_{dif-dis,i}\right) + \left(\sum_{i=1}^{I} \alpha_{im} \mathbf{j}^{m}_{dif-dis,i}\right) \quad (11)$$

where q^{M}_{adv} is the advective velocity and $\mathbf{j}^{L}_{dif-dis,i}$ is the individual diffusive-dispersive flux of each i-th species evaluated at the L-th modeling level. These fluxes are defined by the well-known Nernst–Planck equation based on the assumption that the gradient of the electrochemical potential of each species acts as a driving force for the diffusion-dispersive transport mechanism (Steefel et al., 2015; Masi et al., 2017; Tournassat et al., 2020):

$$\mathbf{j}^{L}_{dif-dis,i} = -u^{L}_{i} c^{L}_{i} \nabla \mu^{L}_{i} \quad (12)$$

where the electrochemical potential of each i-th species, μ^{L}_{i}, is expressed as:

$$\mu^{L}_{i} = \mu_{oi} + RT \ln a^{L}_{i} + z_i F \psi^{L} \quad (13)$$

where, μ_{oi} is the standard electrochemical potential, and ψ^{L} is the electrical potential checked at the corresponding L-th level. This electrical potential could include the electrostatic effects generated by multicomponent diffusion (different transport velocities of species) and related to the imbalance produced by the charge surface of the clays (Appelo and Wersin, 2007). The species mobility, u^{L}_{i}, is proportional to the effective diffusive-dispersive coefficient, $D^{L}_{e,i}$, through the Nernst-Einstein relation (See supplementary material).

Taking into account Eq (13), the diffusive-dispersive flux of each i-th species can be expressed as the sum of the two contributions: (i) Fickian transport driven by a chemical activity gradient and (ii) electromigratory transport induced by an electrical potential gradient:

$$\mathbf{j}^{L}_{dif-dis,i} = -D^{L}_{e,i} c^{L}_{i} \nabla\left(\ln a^{L}_{i}\right) - \frac{z_i F D^{L}_{e,i}}{RT} c^{L}_{i} \nabla \psi^{L} \quad (14)$$

If the clay is not exposed to external electrical potential, then the electrical current is null (Boudreau et al., 2004) and thus $\sum_{i=1}^{I} z_i \mathbf{j}^{L}_{dif-dis,i} = 0$. Considering this aspect, the electrical potential gradient, $\nabla\psi^{L}$, can be expressed according to (Appelo and Wersin, 2007) as:

$$\nabla \psi^{L} = -\frac{\sum_{i=1}^{I} \frac{z_i D^{L}_{i} c^{L}_{i}}{RT} \nabla\left(RT \ln a^{L}_{i}\right)}{\sum_{i=1}^{I} \frac{z_i^2 D^{L}_{i} c^{L}_{i} F}{RT}} \quad (15)$$

2.3.2. Mineral dissolution/precipitation reactions

The sink/source term, f_m, involves any temporal change in species concentration that is not related to transport is of the m-th species. In this model, f_m contemplates the effects produced by mineral dissolution/precipitation reactions by the following expression:

$$f_m = \sum_{j=1}^{J} \alpha_{j\,m}\, r_j \quad (16)$$

where "J" is the number of mineral contemplates in the model, $\alpha_{j\,m}$ is the m-th master species in the dissolution/precipitation reaction of the j-th mineral and r_j is the dissolution/precipitation rate, which is calculated by a general kinetic law provided by Lasaga (1998) and described in López-Vizcaíno et al. (2019) as follows:

$$r_j = \pm k_j\, SSA_j \rho_w \varphi^{M}\, Sr^{M} \left|1 - \Omega_j\right| \left(\frac{m_j}{m_{0,j}}\right) \quad (17)$$

where k_j is the kinetic constant of dissolution (negative value) or precipitation (positive value) of the j-th mineral, SSA_j is the specific surface area, and m_j and $m_{0,j}$ represent the mass of the j-th mineral and the initial value, respectively. Finally, Ω_j is the saturation ratio defined as follows:

$$\Omega_j = \frac{IAP_j}{K_{s,j}} \quad (18)$$

where IAP_j is the ionic activity product and $K_{s,j}$ is the solubility constant of the j-th mineral.

Finally, a balance of mineral mass, m_j, has been included in the model to determine the temporal variation of each j-th mineral, as follows:

$$\frac{dm_j}{dt} = r_j \quad (19)$$

3. Numerical implementation

The numerical model was implemented in COMSOL Multiphysics (COMSOL, 2018), a partial differential equation solver that applies the finite element method with Lagrange multipliers. Instead of relying on preprogrammed modules provided by the software, the authors utilized the "multiphysics" capability of the platform, defining both differential and algebraic equations through constitutive models to account for initial and boundary conditions. The adaptability and versatility of this multiphysics environment allowed for such customizations (Brown et al., 2008; Keyes et al., 2013). In addition, to enhance convergence behavior and maintain solution efficiency while handling more complex problems, the model took advantage of automatic differentiation techniques (Palacios et al., 2013), particularly those provided by COMSOL Multiphysics, which enabled the definition of symbolic expressions for the iteration matrix (Gobbert et al., 2009).

In the proposed model, a total of 27 state variables needed to be solved at each time step. This comprised 10 partial differential equations for the mass balance of master species, 4 ordinary differential equations for the mass balance of the minerals, and 13 algebraic equations for chemical speciation.

The spatial discretization consisted of 100 one-dimensional elements of identical size with a Lagrange linear basis function. The time discretization is based on the Backward Differentiation Formula (BDF) of order 5, employed in the IDA solver (Hindmarsh et al., 2005). Adaptive time-stepping has been employed to adjust the time step to the required resolution tolerances (COMSOL, 2018).

4. Infiltration test description

The verification and validation processes of the proposed model are based on the same experimental test. This test corresponds to a multicomponent advective-diffusive transport experiment in MX-80 compacted bentonite (Fernández et al., 2011; Jenni et al., 2014). The bentonite used in this infiltration test comes from the LOT experiment performed at Äspö, Sweden, specifically of Block 13, which was obtained from Parcel A2 (Karnland et al., 2009). The detailed physico-chemical characterization of this material can be found in Karnland et al. (2009). The experimental setup was designed at the Paul Scherrer Institut (see Fig. 1), and the infiltration test was conducted by the University of Bern. A detailed description of this setup can be found in the literature (Mäder, 2004, 2005). The aim of this test is to extract and analyze the porewater composition of a compacted bentonite and to study the transport of ionic species through its voids. For this purpose, the bentonite column was isolated and confined. A synthetic saline solution was infiltrated by applying a constant hydraulic gradient from

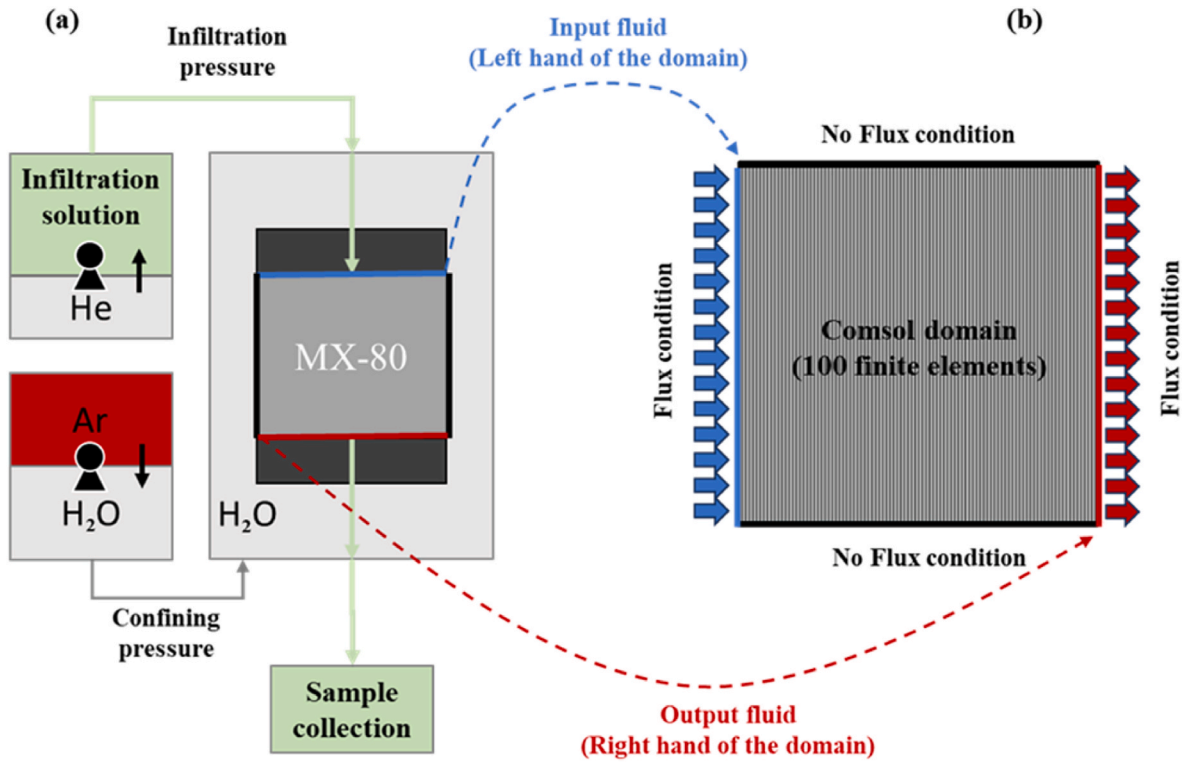

Fig. 1. (a) Schematic of the experimental setup of the infiltration experiment. Adapted from Fernández et al. (2011). (b) Scheme of the used mesh and boundary conditions in the simulations.

one end of the column and the outflow solution was collected at the other end. The porewater extracted from the bentonite sample was collected in a syringe during the fixed observation times. The infiltration and confining pressures are provided by pressurization with helium and argon gases, respectively. The initial composition corresponds to the porewater of compacted bentonite assuming that gypsum and calcite equilibrium is achieved. On the other hand, the composition of the infiltration solution was selected to simulate a natural porewater similar to that present in the host rock at Äspö. The infiltration test was divided into two stages: (i) the first stage had a duration of 300 days, and the (ii) second stage was extended up to 970 days, where the main anion in the infiltration solution, chloride, was changed by nitrate at 216.4 mmol L^{-1} (Fernández et al., 2011; Jenni et al., 2014).

5. Model verification. Benchmarking exercise

The verification of the proposed model has been carried out by a one-dimensional benchmarking exercise based on the fourth benchmark presented by Alt-Epping et al. (2015). This exercise considers (i) the implementation of an electric double layer (Donnan space) induced by a charged bentonite surface, (ii) the transport of species defined by the Nernst−Planck equation and (iii) the surface reactions determined by the Donnan equilibrium. Only Phreeqc (Parkhurst and Appelo, 2013) was selected as reference software to check the results obtained in the benchmarking exercise because the results of the two codes proposed in Alt-Epping et al. (2015) show a good agreement. The input and database used in Phreeqc can be found in the supplementary material.

5.1. General benchmark specification

The sample has a length of 0.05 m. A total volume of 5×10^{-4} m^3 is assumed for the calculations. The simulation exercise reproduces 300 days of the test according with the specification of the benchmark (Alt-Epping et al., 2015) that corresponds only with the first phase of the experiment. In the second phase, the composition of the infiltration fluid was modified by exchanging the main anion Cl^- by $NO3^-$, while the cation concentrations and ionic strength were maintained. Isothermal conditions are assumed (298.15 K). The hydraulic flux, q^{M}_{adv}, applied to the top of the sample corresponds to the left-hand boundary. The hydrodynamic dispersion is considered in the model. The porosity distribution between the macro- and microstructural modeling levels assumed is fixed in Alt-Epping et al. (2015). In the same way, the diffusive transport in the microstructure is despicable compared to the macrostructural level (this assumption is applied through the tortuosity values. The general specifications assumed in the verification process are presented in Table SM4.

5.2. Geochemical system

Master and secondary species and specific parameters such as hard-core diameter and binary diffusion coefficient are presented in Table SM5.

The equilibrium constants, $K_{eq,i}$, are defined by Eq. (SM6) using the fitting parameters shown in Table SM1. The effective diffusive-dispersive coefficients of each species are determined by Eq. (SM8) for both modeling levels.

Table SM6 presents the minerals included in the geochemical system together with associated parameters (molar volume and volume fraction). The SSA value of the reactive minerals has been taken equal to 100 m^2 m^{-3}_{bulk} as it has been reported in (Alt-Epping et al., 2015). The solubility constant, $K_{s,j}$, and the kinetic constant of mineral dissolution-precipitation reactions, k_j, are obtained by Eqs. (SM10) and (SM11), using the fitting parameters provided in Tables SM2 and SM3, respectively. In addition, it is important to remark that montmorillonite is considered an inert material.

The chemical composition of the initial porewater of bentonite and the infiltration solution are presented in Table SM7 (Alt-Epping et al., 2015). Flux conditions were applied in both boundaries considering the composition of the infiltration solution in the left hand of the domain

(input fluid) and the composition of the porewater at each time in the right hand of the domain (output fluid).

5.3. Results of benchmarking

According to the results exposed on the benchmark exercise presented by Alt-Epping et al. (2015), two different evaluations have been carried out. First, the temporal evolution of C_m^M and pH was evaluated at the right hand of the domain, at a distance of 0.05 m, in outflow point (Fig. 2), and second, the spatial distribution of the main species concentration c_i^L was evaluated at the micro- and macrostructural levels after 300 days of simulation (Figure SM2).

The agreement between the results obtained with both models (Comsol and Phreeqc) is very satisfactory in the two evaluations conducted. Based on the results shown in Figure SM2, it is possible to observe the effect of the charged surface of the montmorillonite on the distribution of species between the two modeling levels. The anions are displaced due to the negative charge of the clay, generally increasing its concentration in the macroporosity. On the other hand, the concentration of cations is higher in the microporosity due to the electrostatic attraction produced by the bentonite surface.

6. Model validation and discussion

The first simulation conducted in the validation process contemplates a similar parametrization to that in the verification process, except the value of infiltration flux that in this case is 2.3×10^{-9} m^3 m^{-2} s^{-1}. This value is extracted by Alt-Epping et al. (2015), which is calculated from the experimental data presented in Fernández et al. (2011). The numerical results obtained in this simulation compared with the experimental results of the infiltration test can be found in Fig. 3.

Analyzing Fig. 3, it can be noted that the simulated behavior of the total concentration of the main master species presents a similar trend to the experimental results, i.e., good qualitative agreement, even if no mechanical effects resulting from changes in the initial confining pressure are taken into account. However, from a quantitative point of view, discrepancies are observed. A great difference between the initial concentration of the pore water is observed. The initial composition of porewater was determined by Fernández et al. (2011) based on the measured composition of exchange sites and the assumption of initial gypsum and calcite equilibrium (see Table SM7). The determination of an "average" initial composition is a very difficult task due to the nonhomogeneous distribution of minerals and other species in the sample (extracted from the LOT experiment) before the infiltration experiment (Jenni et al., 2014). Considering this, a new set of initial concentrations of the species present in the pore water is recommended (Table SM8). For this, values are proposed that are consistent with the experimentally observed trends and maintain the assumption carried out by Fernández et al. (2011) (the concentration of gypsum and calcite is in equilibrium with the porewater).

Two new simulations were conducted using the proposed new chemical composition of the initial bentonite porewater composition. The first simulation maintaining the same set of parameters that were used previously in the model and the second simulation optimizing two variables: the tortuosity of the macrostructural level ($\tau^M = 0.35$) and the dispersivity ($D_{dis} = 0.005$ m). Tortuosity and dispersivity are the only parameters used for the curve fitting as they have the highest degree of uncertainty. The results are presented in Fig. 4a and b, respectively.

The numerical results obtained by applying the adjusted chemical composition of the initial bentonite porewater composition and invariably maintaining the parametrization (Fig. 4a) present a significant improvement in the agreement with the experimental results. However, the agreement is much more satisfactory when using the optimized values of $\tau^M = 0.35$ and $D_{dis} = 0.005$ (Fig. 4b).

To qualitatively analyze the obtained results, it is necessary to first examine the evolution of sulfate over time. A characteristic trend of the total concentration of the SO_4^{2-} component evaluated in the outflow stream is observed. An increase in sulfate concentration is observed up to approximately 75 days of testing, and then a decreasing evolution is observed. Even so, the sulfate concentration at the output of the bentonite sample is always higher than the infiltrated concentration: 2.02×10^{-3} mol kg_w^{-1}. This behavior is in accordance with the dissolution of gypsum (Fernández et al., 2011; Jenni et al., 2014; Alt-Epping et al., 2015). Figure SM2 presents an analysis of the temporal evolution

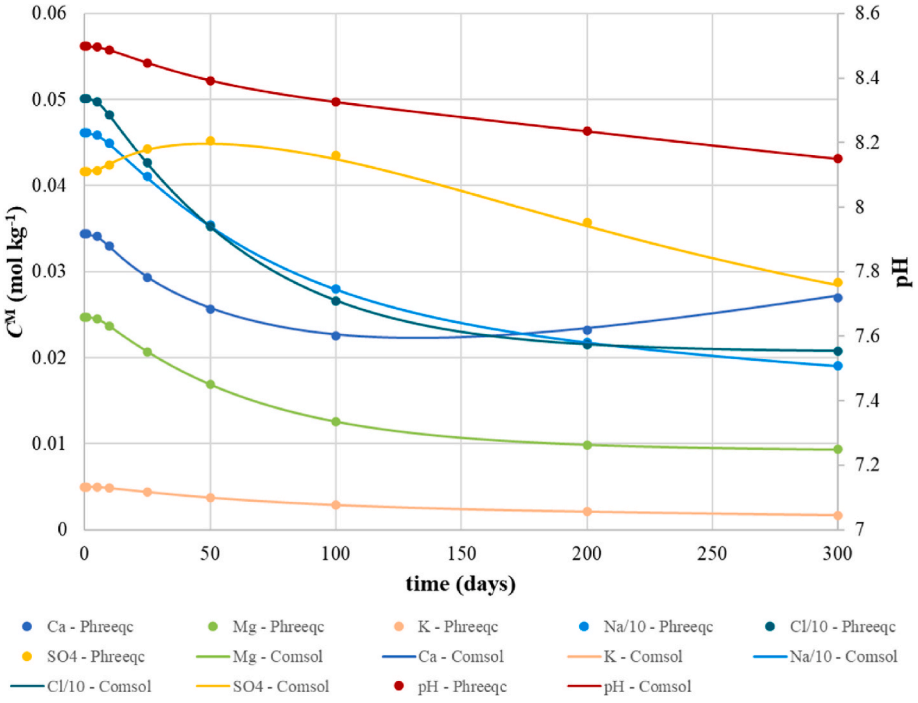

Fig. 2. Temporal evolution of the computed total concentration of the main master species and pH evaluated at the outflow point at 0.05 m. Solid line: COMSOL results and markers: Phreeqc results.

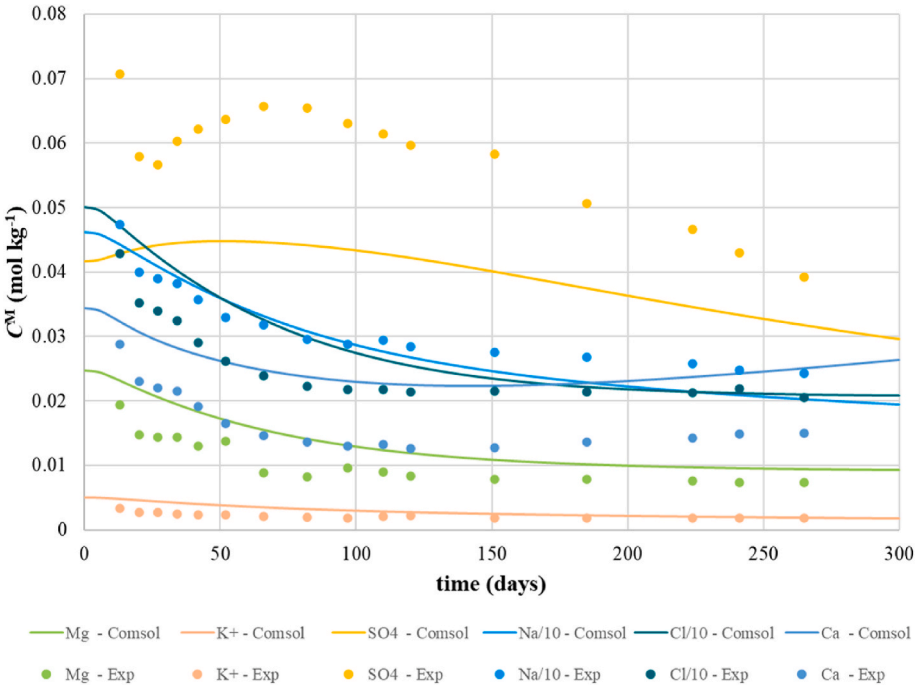

Fig. 3. Temporal evolution of the total concentration of the main master species evaluated at the outflow point. Solid line: COMSOL results and markers: Experimental results from Fernández et al. (2011).

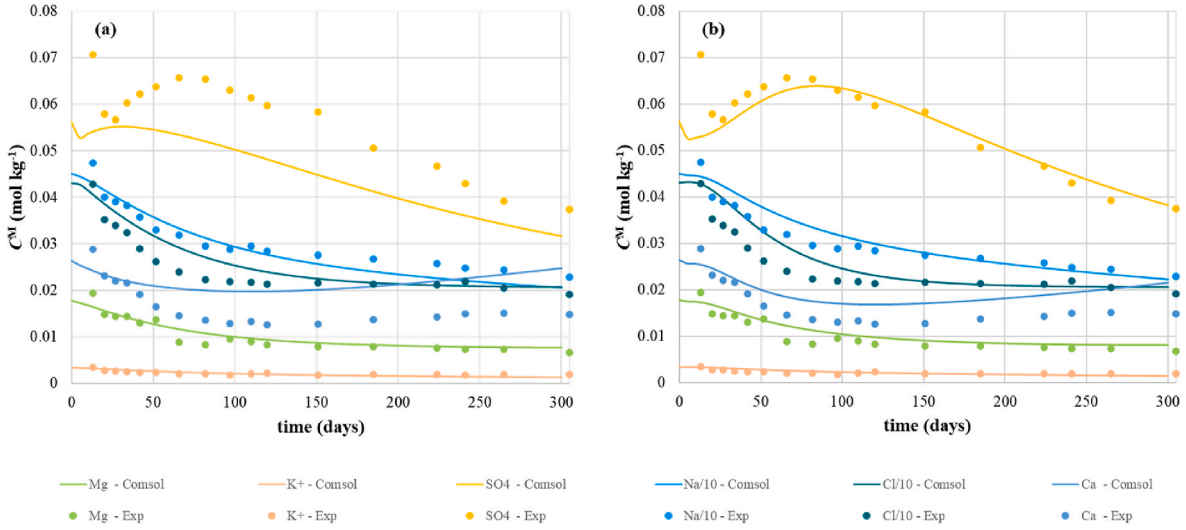

Fig. 4. Temporal evolution of the total concentration of the main master species evaluated at the outflow point. Solid line: COMSOL results and markers: Experimental results from Fernández et al. (2011). (a) $\tau^M = 1$ and $D_{dis} = 0.05$ y and (b) $\tau^M = 0.35$ and $D_{dis} = 0.005$.

and spatial distribution of the gypsum concentration. Figure SM2a shows the spatial profiles of a normalized gypsum concentration, as the ratio between the concentration at each time and the initial concentration. This variable indicates the progressive dissolution process of this mineral. Consequently, the average mass of the gypsum in the sample is reduced as the experiment progresses (Figure SM2b). As the gypsum precipitation process has been confirmed, one would expect the evolution of the Ca^{2+} concentration in the outflow to have a similar tendency to that of the sulfate. However, Fig. 4b shows that the tendency is different. A drop in the concentration is observed in the initial stage of the experiment, always remaining below the concentration fixed in the infiltration solution: 5.84×10^{-2} mol kg_w^{-1}. In this context, it is important to highlight that the concentrations of Na^+, Mg^{2+} and K^+ in the outflow are higher than those in the infiltration solution (Fig. 5a).

These aspects could be related to a cation exchange process where Ca^{2+} fills exchanger sites and displaces the Na^+ (which dominates the exchanger sites of the bentonite surface at the beginning of the infiltration test), Mg^{2+} and K^+ species. To check this assumption, the charge equivalents (eq m^{-3}) provided by each component in the microstructure were estimated. This approach for the determination of the positions occupied by the exchange ions has been used previously and confirmed experimentally (Alt-Epping et al., 2018), obtaining consistent estimates of ion exchange composition. The values obtained in Fig. 5b could be a good marker to illustrate which species and to what extent it is available at the microstructural level to fill exchange positions in the bentonite.

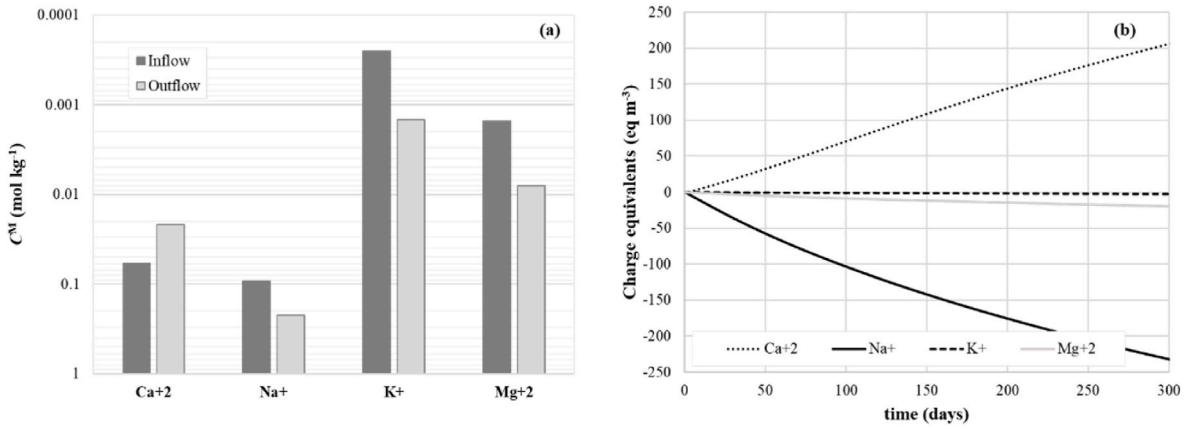

Fig. 5. Simulated results. (a) Concentration of Ca^{2+}, Na^{+}, Mg^{2+} and K^{+} in the inflow and outflow evaluated at 300 days. (b) Temporal evolution of the cumulative charge equivalents (eq m^{-3}) provided by Ca^{2+}, Na^{+}, Mg^{2+} and K^{+} at the microstructural level.

7. Conclusions

The proposed reactive transport model for bentonites presents satisfactory results. The verification process has been successfully completed, obtaining a perfect correspondence between the results produced by the proposed model and those obtained with the reference software (Phreeqc). On the other hand, the simulation exercise focused on the validation of the code has also shown good agreement with the experimental results. However, there are several discrepancies between the numerical and experimental responses. At this point, it is important to highlight that the model does not consider the mechanical changes of the samples produced mainly by the application of a nonconstant confining pressure at the start of the test. Taking into account this limitation, the results obtained with the proposed model are very promising, but even more so if it is considered that having used a multiphysics environment (COMSOL) as an implementation platform, the future coupling of a mechanical module is totally feasible. This task is currently under development as a result of the previous works of the authors in this field of study (Navarro et al., 2019). Notwithstanding this, our firm conviction is that the validation of a numerical model is an ongoing and flexible undertaking, which should be extended to its utmost limits to attain the highest level of accuracy and code quality. Consequently, additional modeling endeavors are imperative to precisely depict such complex systems and to understand and quantitatively elucidate the experimental findings presented by fellow researchers investigating bentonites.

CRediT authorship contribution statement

Virginia Cabrera: Formal analysis, Validation, Writing – original draft. **Rubén López-Vizcaíno:** Conceptualization, Formal analysis, Funding acquisition, Methodology, Validation, Writing – original draft, Writing – review & editing. **Ángel Yustres:** Conceptualization, Funding acquisition, Methodology, Writing – review & editing. **Vicente Navarro:** Funding acquisition, Project administration, Supervision, Writing – review & editing.

Declaration of competing interest

The authors declare that they have no known competing financial interests or personal relationships that could have appeared to influence the work reported in this paper.

Data availability

Data will be made available on request.

Acknowledgments

The authors acknowledge funding support from (i) grant [BIA2017–89287-R] co-funded by MCIN/AEI/10.13039/501100011033 and by " ERDF A way of making Europe", (ii) grant [PID2020–118291RB-I00] funded by MCIN/AEI/10.13039/501100011033and (iii) Postdoctoral grant [2022-POST-20890] co-funded by University of Castilla-La Mancha and European Social Fund plus (ESF+).

Appendix A. Supplementary data

Supplementary data to this article can be found online at https://doi.org/10.1016/j.chemosphere.2023.141050.

References

Alonso, E.E., Navarro, V., 2005. Microstructural model for delayed deformation of clay: Loading history effects. Can. Geotech. J. 42, 381–392. https://doi.org/10.1139/t04-097.

Alonso, E.E., Vaunat, J., Gens, A., 1999. Modelling the mechanical behaviour of expansive clays. Eng. Geol. 54, 173–183. https://doi.org/10.1016/S0013-7952(99)00079-4.

Alt-Epping, P., Gimmi, T., Wersin, P., Jenni, A., 2018. Incorporating electrical double layers into reactive-transport simulations of processes in clays by using the Nernst-Planck equation: a benchmark revisited. Appl. Geochem. 89, 1–10. https://doi.org/10.1016/j.apgeochem.2017.10.018.

Alt-Epping, P., Tournassat, C., Rasouli, P., Steefel, C.I., Mayer, K.U., Jenni, A., Mäder, U., Sengor, S.S., Fernández, R., 2015. Benchmark reactive transport simulations of a column experiment in compacted bentonite with multispecies diffusion and explicit treatment of electrostatic effects. Comput. Geosci. 19, 535–550. https://doi.org/10.1007/s10596-014-9451-x.

Appelo, C.A.J., Wersin, P., 2007. Multicomponent diffusion modeling in clay systems with application to the diffusion of Tritium, Iodide, and Sodium in Opalinus clay. Environ. Sci. Technol. 41, 5002–5007. https://doi.org/10.1021/es0629256.

Arcos, D., Grandia, F., Domenech, C., Fernandez, A.M., Villar, M.V., Muurinen, A., Carlsson, T., Sellin, P., Hernan, P., 2008. Long-term geochemical evolution of the near field repository: insights from reactive transport modelling and experimental evidences. J. Contam. Hydrol. 102, 196–209. https://doi.org/10.1016/j.jconhyd.2008.09.021.

Barry, D.A., Miller, C.T., Culligan, P.J., Bajracharya, K., 1997. Analysis of split operator methods for nonlinear and multispecies groundwater chemical transport models. Math. Comput. Simulat. 43, 331–341. https://doi.org/10.1016/S0378-4754(97)00017-7.

Bethke, C.M., 2007. Geochemical and Biogeochemical Reaction Modeling. Cambridge University Press.

Bildstein, O., Claret, F., 2015. Chapter 5 - stability of clay barriers under chemical Perturbations. In: Tournassat, C., Steefel, C.I., Bourg, I.C., Bergaya, F. (Eds.), Developments in Clay Science. Elsevier, pp. 155–188.

Bildstein, O., Claret, F., Frugier, P., 2019. RTM for waste repositories. Rev. Mineral. Geochem. 85, 419–457. https://doi.org/10.2138/rmg.2019.85.14.

Boudreau, B.P., Meysman, F.J.R., Middelburg, J.J., 2004. Multicomponent ionic diffusion in porewaters: Coulombic effects revisited. Earth Planet Sci. Lett. 222, 653–666. https://doi.org/10.1016/j.epsl.2004.02.034.

Brown, D.L., Bell, J., Estep, D., Gropp, W., Hendrickson, B., Keller-McNulty, S., Keyes, D., Oden, J.T., Petzold, L., Wright, M., 2008. Applied Mathematics at the U.S.

Department of Energy: Past, present and a view to the future. Applied Mathematics at the U.S. Department of Energy: Past, Present and a View to the Future.
Carrayrou, J., Mosé, R., Behra, P., 2004. Operator-splitting procedures for reactive transport and comparison of mass balance errors. J. Contam. Hydrol. 68, 239–268. https://doi.org/10.1016/S0169-7722(03)00141-4.
Claret, F., Marty, N., C.M, Debure, M., Linard, Y., Tournassat, C., 2018. Modeling the long-term stability of multi-barrier systems for radioactive waste disposal in geological clay formations. In: Yitian, X., Fiona, W., Tianfu, X., Carl, S. (Eds.), Reactive Transport Modeling: Applications in Subsurface Energy and Environmental Problems. CHAPTER 8.
COMSOL, 2018. COMSOL Multiphysics Reference Manual Version, 5.4. COMSOL.
Daveler, S.A., Wolery, T.J., 1992. In: L.-U.-M.-P (Ed.), EQPT, A Data File Preprocessor for the EQ3/6 Software Package–User's Guide and Related Documentation (Version 7.0). in: II. Lawrence Livermore National Laboratory, University of California, Livermore, California.
Deissmann, G., Ait Mouheb, N., Martin, C., Turrero, M.J., Torres, E., Kursten, B., Weetjens, E., Jacques, D., Cuevas, J., Samper, J., Montenegro, L., Leivo, M., Somervuori, M., Carpen, L., 2021. Experiments and Numerical Model Studies on Interfaces.
Delay, J., Bossart, P., Ling, L., Blechschmidt, I., Ohlsson, M., Vinsot, A., Nussbaum, C., Maes, N., 2014. Three decades of underground research laboratories: what have we learned? Geological Society, London, Special Publications 400, 7–32. https://doi.org/10.1144/SP400.1.
Drummond, S.E., 1981. Boiling and Mixing of Hydrothermalfluids: Chemical Effects on Mineral Precipitation. Pennsylvania State University.
Farrell, P.E., Ham, D.A., Funke, S.W., Rognes, M.E., 2013. Automated Derivation of the Adjoint of High-Level Transient Finite Element Programs, vol. 35, pp. C369–C393. https://doi.org/10.1137/120873558.
Fernández, R., Mäder, U., Jenni, A., 2011. Multi-Component Advective-Diffusive Transport Experiment in MX-80 Compacted Bentonite: Method and Results of 1st Phase of Experiment. Working Report NAB 11-02. Nagra.
Gens, A., Alonso, E.E., 1992. A framework for the behaviour of unsaturated expansive clays. Can. Geotech. J. 29, 1013–1032. https://doi.org/10.1139/t92-120.
Gimmi, T., Alt-Epping, P., 2018. Simulating Donnan equilibria based on the Nernst-Planck equation. Geochem. Cosmochim. Acta 232, 1–13. https://doi.org/10.1016/j.gca.2018.04.003.
Gobbert, M.K., Churchill, A., Wang, G., Seidman, T.I., 2009. COMSOL Multiphysics for efficient solution of a transient reaction-diffusion system with fast reaction. In: Rao, Y. (Ed.), COMSOL Conference 2009 Boston, USA.
Hindmarsh, A.C., Brown, P.N., Grant, K.E., Lee, S.L., Serban, R., Shumaker, D.E., Woodward, C.S., 2005. SUNDIALS: Suite of nonlinear and differential/algebraic equation solvers. ACM Trans. Math. Softw. 31, 363–396. https://doi.org/10.1145/1089014.1089020.
Houston, P., Sime, N., 2018. Automatic symbolic computation for Discontinuous. Galerkin Finite Element Methods 40, C327–C357. https://doi.org/10.1137/17m1129751.
Hueckel, T.A., 1992. Water-mineral interaction in hygromechanics of clays exposed to environmental loads: a mixture-theory approach. Can. Geotech. J. 29, 1071–1086. https://doi.org/10.1139/t92-124.
IAEA, 2020. Design Principles and Approaches for Radioactive Waste Repositories. INTERNATIONAL ATOMIC ENERGY AGENCY, Vienna.
Jacques, D., Šimůnek, J., Mallants, D., van Genuchten, M.T., 2006. Operator-splitting errors in coupled reactive transport codes for transient variably saturated flow and contaminant transport in layered soil profiles. J. Contam. Hydrol. 88, 197–218. https://doi.org/10.1016/j.jconhyd.2006.06.008.
Jenni, A., Mäder, U., Fernández, R., 2014. Multi-component Advective-Diffusive Transport Experiment in MX-80 Compacted Bentonite: Method and Results of 2nd Phase of Experiment and Post Mortem Analysis. Working Report NAB 14-22. Nagra.
Karnland, O., Muurinen, A., Karlsson, F., 2005. Bentonite swelling pressure in NaCl solutions - experimentally determined data and model calculations. In: Advances in Understanding Engineered Clay Barriers - Proceedings of the International Symposium on Large Scale Field Tests in Granite, pp. 241–256.
Karnland, O., Olsson, S., Dueck, A., Birgersson, M., Nilsson, U., Hernan-Hakansson, T., Pedersen, K., Nilsson, S., Eriksen, T., Rosborg, B., 2009. Long Term Test of Buffer Material at the Äspö Hard Rock Laboratory, LOT Project. Final Report on the A2 Test Parcel. SKB Technical Report TR-09-29. https://www.skb.se/publikation/1961944/TR-09-29.pdf.
Karnland, O., Olsson, S., Nilsson, U., 2006. Mineralogy and Sealing Properties of Various Bentonites and Smectite-Rich Clay Materials. SKB Technical Report TR-06-30. https://skb.se/upload/publications/pdf/TR-06-30.pdf.
Keyes, D.E., McInnes, L.C., Woodward, C., Gropp, W., Myra, E., Pernice, M., Bell, J., Brown, J., Clo, A., Connors, J., Constantinescu, E., Estep, D., Evans, K., Farhat, C., Hakim, A., Hammond, G., Hansen, G., Hill, J., Isaac, T., Jiao, X., Jordan, K., Kaushik, D., Kaxiras, E., Koniges, A., Lee, K., Lott, A., Lu, Q., Magerlein, J., Maxwell, R., McCourt, M., Mehl, M., Pawlowski, R., Randles, A.P., Reynolds, D., Rivière, B., Rüde, U., Scheibe, T., Shadid, J., Sheehan, B., Shephard, M., Siegel, A., Smith, B., Tang, X., Wilson, C., Wohlmuth, B., 2013. Multiphysics simulations: Challenges and opportunities. Int. J. High Perform. Comput. Appl. 27, 4–83. https://doi.org/10.1177/1094342012468181.
Kiviranta, L., Kumpulainen, S., 2011. In: Workreport, P. (Ed.), Quality Control and Characterization of Bentonite Materials. POSIVA.
Kiviranta, L., Kumpulainen, S., Pintado, X., Karttunen, P., Schatz, T., 2018. In: P.W (Ed.), Characterization of Bentonite and Clay Materials 2012-2015. in: 2016-05. POSIVA.
Lasaga, A.C., 1998. Kinetic Theory in the Earth Sciences. Princeton University Press, Princeton, NJ, USA.
Lichtner, P.C., 2007. FLOTRAN Users Manual: Two-phase Nonisothermal Coupled Thermal-Hydrologic-Chemical (THC) Reactive Flow and Transport Code. Los Alamos National Laboratory, Los Alamos, New Mexico.
López-Vizcaíno, R., dos Santos, E.V., Yustres, A., Rodrigo, M.A., Navarro, V., Martínez-Huitle, C.A., 2019. Calcite buffer effects in electrokinetic remediation of clopyralid-polluted soils. Separation and Purification Technology 212, 376–387. https://doi.org/10.1016/j.seppur.2018.11.034.
López-Vizcaíno, R., Yustres, Á., Cabrera, V., Navarro, V., 2021. A worksheet-based tool to implement reactive transport models in COMSOL Multiphysics. Chemosphere 266, 129176. https://doi.org/10.1016/j.chemosphere.2020.129176.
López-Vizcaíno, R., Yustres, A., León, M.J., Saez, C., Cañizares, P., Rodrigo, M.A., Navarro, V., 2017. Multiphysics implementation of electrokinetic remediation models for natural soils and porewaters. Electrochim. Acta 225, 93–104. https://doi.org/10.1016/j.electacta.2016.12.102.
Mäder, U., 2004. Porewater Chemistry (PC) Experiment: A New Method of Porewater Extrac Tion from Opalinus Clay with Results for a Sample from Borehole BPC-A1. Mont Terri Technical Note TN 2002-25.
Mäder, U., 2005. Porewater chemistry, porosity and hydraulic conductivity of Callovo Oxfordian claystone at the EST-322 deep drilling site sampled by the method of advective displacement (Laboratoire de Rechereche Souterrain de Meuse/Haute-Marne). Nagra Working Report NAB 05-04. Nagra.
Masi, M., Ceccarini, A., Iannelli, R., 2017. Multispecies reactive transport modelling of electrokinetic remediation of harbour sediments. J. Hazard Mater. 326, 187–196. https://doi.org/10.1016/j.jhazmat.2016.12.032.
Mašín, D., 2013. Double structure hydromechanical coupling formalism and a model for unsaturated expansive clays. Eng. Geol. 165, 73–88. https://doi.org/10.1016/j.enggeo.2013.05.026.
Mayer, K.U., 2010. MIN3P User Guide. University of British Columbia, Department of 413 Earth and Ocean Sciences.
McRae, A.T.T., Bercea, G.-T., Mitchell, L., Ham, D.A., Cotter, C.J., 2016. Automated generation and symbolic Manipulation of Tensor product finite. Elements 38, S25–S47. https://doi.org/10.1137/15m1021167.
Navarro, V., Asensio, L., De la Morena, G., Pintado, X., Yustres, Á., 2015. Differentiated intra-and inter-aggregate water content models of mx-80 bentonite. Appl. Clay Sci. 118, 325–336. https://doi.org/10.1016/j.clay.2015.10.015.
Navarro, V., Asensio, L., Gharbieh, H., De la Morena, G., Pulkkanen, V.-M., 2019. Development of a multiphysics numerical solver for modeling the behavior of clay-based engineered barriers. Nucl. Eng. Technol. 51, 1047–1059. https://doi.org/10.1016/j.net.2019.02.007.
Palacios, F., Alonso, J., Duraisamy, K., Colonno, M., Hicken, J., Aranake, A., Campos, A., Copeland, S., Economon, T., Lonkar, A., Lukaczyk, T., Taylor, T., 2013. Stanford University Unstructured (SU2): an open-source integrated computational environment for multi-physics simulation and design. In: 51 St AIAA Aerospace Sciences Meeting Including the New Horizons Forum and Aerospace Exposition.
Parkhurst, D.L., Appelo, C.A.J., 2013. In: Survey, U.S.G. (Ed.), Description of Input and Examples for PHREEQC Version 3—A Computer Program for Speciation, Batch-Reaction, One-Dimensional Transport, and Inverse Geochemical Calculations, p. 497. Denver, USA.
Posiva, 2012a. Safety Case for the Disposal of Spent Nuclear Fuel at Olkiluoto - Features, Events and Processes.
Posiva, 2012b. Safety Case for the Disposal of Spent Nuclear Fuel at Olkiluoto - Performance Assessment.
Pusch, R., 1992. Use of bentonite for isolation of radioactive waste products. Clay Miner. 27, 353–361. https://doi.org/10.1180/claymin.1992.027.3.08.
Pusch, R., 2006. The performance of clay barriers in repositories for high-level radioactive waste. Nucl. Eng. Technol. 38, 483–488.
Rasouli, P., Steefel, C.I., Mayer, K.U., Rolle, M., 2015. Benchmarks for multicomponent diffusion and electrochemical migration. Comput. Geosci. 19, 523–533. https://doi.org/10.1007/s10596-015-9481-z.
Rolle, M., Sprocati, R., Masi, M., Jin, B., Muniruzzaman, M., 2018. Nernst-Planck-based description of transport, Coulombic interactions, and geochemical reactions in porous media: modeling approach and benchmark experiments. Water Resour. Res. 54, 3176–3195. https://doi.org/10.1002/2017WR022344.
Romero, E., 2013. A microstructural insight into compacted clayey soils and their hydraulic properties. Eng. Geol. 165, 3–19. https://doi.org/10.1016/j.enggeo.2013.05.024.
Romero, E., Della Vecchia, G., Jommi, C., 2011. An insight into the water retention properties of compacted clayey soils. Geotechnique 61, 313–328. https://doi.org/10.1680/geot.2011.61.4.313.
Romero, E., Gens, A., Lloret, A., 1999. Water permeability, water retention and microstructure of unsaturated compacted Boom clay. Eng. Geol. 54, 117–127. https://doi.org/10.1016/S0013-7952(99)00067-8.
Sánchez, M., Gens, A., do Nascimento Guimarães, L., Olivella, S., 2005. A double structure generalized plasticity model for expansive materials. Int. J. Numer. Anal. Methods GeoMech. 29, 751–787. https://doi.org/10.1002/nag.434.
Sellin, P., Leupin, O.X., 2014. The use of clay as an engineered barrier in radioactive-waste management - a review. Clay Clay Miner. 61, 477–498. https://doi.org/10.1346/CCMN.2013.0610601.
Sprocati, R., Masi, M., Muniruzzaman, M., Rolle, M., 2019. Modeling electrokinetic transport and biogeochemical reactions in porous media: a multidimensional Nernst–Planck–Poisson approach with PHREEQC coupling. Adv. Water Resour. 127, 134–147. https://doi.org/10.1016/j.advwatres.2019.03.011.
Steefel, C.I., Appelo, C.A.J., Arora, B., Jacques, D., Kalbacher, T., Kolditz, O., Lagneau, V., Lichtner, P.C., Mayer, K.U., Meeussen, J.C.L., Molins, S., Moulton, D., Shao, H., Šimůnek, J., Spycher, N., Yabusaki, S.B., Yeh, G.T., 2015. Reactive

transport codes for subsurface environmental simulation. Comput. Geosci. 19, 445–478. https://doi.org/10.1007/s10596-014-9443-x.
Toprak, E., Olivella, S., Pintado, X., Mokni, N., 2013. Thermo-Hydro-Mechanical Modelling of Buffer. Synthesis Report. POSIVA, 2012-47 (ISBN 987-951-652-229-9).
Tournassat, C., Appelo, C.A.J., 2011. Modelling approaches for anion-exclusion in compacted Na-bentonite. Geochem. Cosmochim. Acta 75, 3698–3710. https://doi.org/10.1016/j.gca.2011.04.001.
Tournassat, C., Steefel, C.I., Gimmi, T., 2020. Solving the Nernst-Planck equation in Heterogeneous porous media with finite volume methods: Averaging approaches at Interfaces. Water Resour. Res. 56 https://doi.org/10.1029/2019wr026832.
Villar, M.V., Romero, E., Lloret, A., 2005. Thermo-mechanical and geochemical effects on the permeability of high-density clays. In: Advances in Understanding Engineered Clay Barriers - Proceedings of the International Symposium on Large Scale Field Tests in Granite, pp. 177–191.
Wersin, P., Kiczka, M., Koskinen, K., 2016. Porewater chemistry in compacted bentonite: application to the engineered buffer barrier at the Olkiluoto site. Appl. Geochem. 74, 165–175. https://doi.org/10.1016/j.apgeochem.2016.09.010.
Yustres, Á., López-Vizcaíno, R., Cabrera, V., Rodrigo, M.A., Navarro, V., 2020. Donnan-ion hydration model to estimate the electroosmotic permeability of clays. Electrochim. Acta 355. https://doi.org/10.1016/j.electacta.2020.136758.
Zhu, C.-M., Ye, W.-M., Chen, Y.-G., Chen, B., Cui, Y.-J., 2013. Influence of salt solutions on the swelling pressure and hydraulic conductivity of compacted GMZ01 bentonite. Eng. Geol. 166, 74–80. https://doi.org/10.1016/j.enggeo.2013.09.001.